Probing the Mechanism of Staphylococcal Nuclease with Unnatural Amino Acids: Kinetic and Structural Studies

J. Kevin Judice, Theresa R. Gamble, Elizabeth C. Murphy, Abraham M. de Vos, Peter G. Schultz*

Staphylococcal nuclease is an enzyme with enormous catalytic power, accelerating phosphodiester bond hydrolysis by a factor of 10^{16} over the spontaneous rate. The mechanistic basis for this rate acceleration was investigated by substitution of the active site residues Glu^{43}, Arg^{35}, and Arg^{87} with unnatural amino acid analogs. Two Glu^{43} mutants, one containing the nitro analog of glutamate and the other containing homoglutamate, retained high catalytic activity at pH 9.9, but were less active than the wild-type enzyme at lower pH values. The x-ray crystal structure of the homoglutamate mutant revealed that the carboxylate side chain of this residue occupies a position and orientation similar to that of Glu^{43} in the wild-type enzyme. The increase in steric bulk is accommodated by a backbone shift and altered torsion angles. The nitro and the homoglutamate mutants display similar pH versus rate profiles, which differ from that of the wild-type enzyme. Taken together, these studies suggest that Glu^{43} may not act as a general base, as previously thought, but may play a more complex structural role during catalysis.

The proposed mechanism of catalysis by staphylococcal nuclease (SNase) is based on high-resolution x-ray crystal structures (*1*, *2*) as well as a series of mechanistic studies (*3*). Glu^{43} is postulated to act as a general base to activate a water molecule for attack on the phosphodiester bond, resulting in a trigonal bipyramidal transition state that is stabilized by interactions with Arg^{87}, Arg^{35}, and the Ca^{2+} ion (Fig. 1). Arg^{87} may also act as a general acid to protonate the 5′-hydroxyl leaving group. Although mutagenesis studies have shown that these residues are important in catalysis, the structural bases for their functions have not yet been clearly defined, largely because substitutions with other naturally occurring amino acids not only reduce catalytic activity, but also alter the protein structure. For example, substitution of Glu^{43} with aspartate leads to a 300-fold reduction in catalytic efficiency (*4*) as well as structural perturbations in the loop adjacent to Glu^{43} (*5*, *6*). Likewise, mutation of either Arg^{87} or Arg^{35} to lysine results in large decreases in catalytic efficiency and changes in protein structure (*7*).

In order to more precisely evaluate the role of Glu^{43} during turnover, we substituted this residue with its nitro analog, S-4-nitro-2-aminobutyric acid (NABA, Fig. 2). Although the nitro group is both isoelectronic and isosteric to the carboxylate group, it is a much poorer base; the pK_a's of the conjugate acids CH_3CO_2H and $CH_3NO_2H^+$ are 4 and −12, respectively (*8*). The geometric requirements for catalysis were probed by comparison of the homologous series homoglutamate (ADPA), glutamate, and aspartate. The Glu^{43}→S-2-amino-5-hydroxypentanoic acid (AHPA) mutant was also generated, in which the carboxylate group of Glu^{43} was substituted with the weakly basic hydroxymethylene group ($pK_a \approx -3$) (*8*). The catalytic roles of Arg^{35} and Arg^{87} were investigated by replacement of these residues with aminoethylhomocysteine (AEHC) and citrulline (CIT). These substitutions were designed to assess the relative contributions of both electrostatic interactions and monodentate as compared with bidentate hydrogen bonding ability to catalysis.

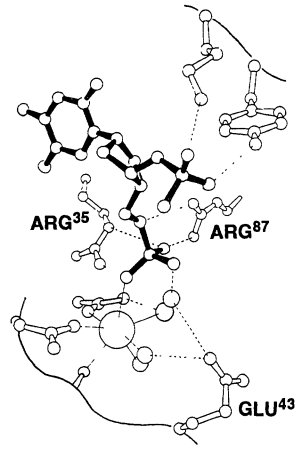

Fig. 1. The active site of staphylococcal nuclease complexed with Ca^{2+} (large sphere) and the inhibitor thymidine 3′,5′-bisphosphate (black) (*2*). Also shown are two water molecules (overlapping small spheres) thought to be candidates for the attacking nucleophile.

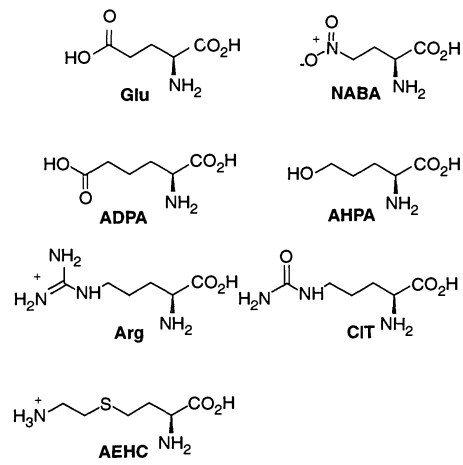

Fig. 2. Amino acids incorporated at the active site of staphylococcal nuclease (*27*).

Incorporation of unnatural amino acids into SNase was accomplished by in vitro suppression of nonsense mutations (TAG) with a chemically aminoacylated suppressor tRNA (*9*, *10*). In vitro expression of SNase from the plasmid pKJSN1, in which the gene for wild-type SNase is under the transcriptional control of the T7 promoter (*11*, *12*), afforded approximately 20 μg of protein per milliliter of reaction mixture with wild-type activity. Addition of suppressor tRNAs aminoacylated (*10*) with the unnat-

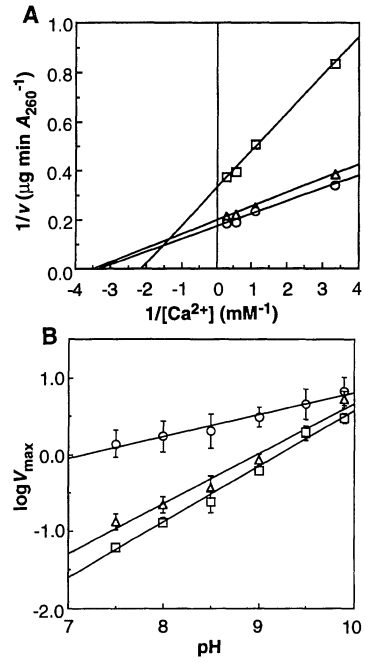

Fig. 3. (**A**) Lineweaver-Burk plots used to determine apparent V_{max} and $K_m^{Ca^{2+}}$ values of wild-type SNase (○) and the Glu^{43}→NABA (□) and Glu^{43}→ADPA (△) mutants. (**B**) The pH dependence of the apparent V_{max} for wild-type SNase (○) and the Glu^{43}→NABA (□) and Glu^{43}→ADPA (△) mutants.

J. K. Judice, E. C. Murphy, P. G. Schultz, Department of Chemistry, University of California, Berkeley, CA 94720.
T. R. Gamble, Graduate Group in Biophysics, University of California, San Francisco, San Francisco, CA 94143, and Department of Protein Engineering, Genentech, Inc., South San Francisco, CA 94080.
A. M. de Vos, Department of Protein Engineering, Genentech, Inc., South San Francisco, CA 94080.
*To whom correspondence should be addressed.

ural amino acids to in vitro protein synthesis reactions programmed with the Arg^{35}, Arg^{87}, or Glu^{43}→nonsense mutant plasmids (*13*) produced mutant proteins with suppression efficiencies between 15 and 40%. Mutant proteins were initially screened for catalytic activity with the use of a chromogenic plate assay (*14*). In contrast to the previously studied mutants at position 43, both the Glu^{43}→NABA and Glu^{43}→ADPA mutants were found to have high hydrolytic activity. The catalytic efficiency of the Glu^{43}→AHPA mutant was reduced by a factor of at least 10^3 relative to that of the wild-type enzyme and was not further studied.

The Glu^{43}→NABA and Glu^{43}→ADPA proteins were purified to homogeneity by ion exchange chromatography (*15*), and their kinetic properties at pH 9.9 were determined (*16*) by spectrophotometric assay (*17*) (Fig. 3A). The kinetic constants of the Glu^{43}→NABA [V_{max} = 3.0 ± 0.5 A_{260} min^{-1} μg^{-1}, Michaelis constant for DNA (K_m^{DNA}) = 26 ± 8 μg/ml] and Glu^{43}→ADPA (V_{max} = 5.2 ± 0.2, K_m^{DNA} = 10 ± 2) were markedly close to those determined for wild-type SNase (V_{max} = 6.7 ± 0.7, K_m^{DNA} = 8 ± 3). Moreover, the K_m values for Ca^{2+} in all three proteins were similar [$K_m^{Ca^{2+}}$ (wild type) = 320 ± 30 μM, $K_m^{Ca^{2+}}$ (Glu^{43}→ADPA) = 290 ± 30, $K_m^{Ca^{2+}}$ (Glu^{43}→NABA) = 470 ± 40], suggesting that there were no significant changes in the Ca^{2+} binding sites of the mutants. The pH dependence of the V_{max} values of both the nitro and homoglutamate mutants was similar and differs from that of the wild-type enzyme (Fig. 3B); for both mutants, V_{max} was proportional to $log[OH^-]^{0.6}$, whereas for the wild-type enzyme V_{max} was proportional to $log[OH^-]^{0.3}$.

The high catalytic activity of the Glu^{43}→NABA mutant was surprising, in light of the poor basicity of this residue and the low activity of the structurally similar Glu^{43}→Gln mutant (*4*). The possibility of a nitronate anion participating as a general base was considered (pK_a = 9 for $CH_3CH_2NO_2$→$CH_3CHNO_2^-$) (*18*), but the similarity of the pH versus rate profiles

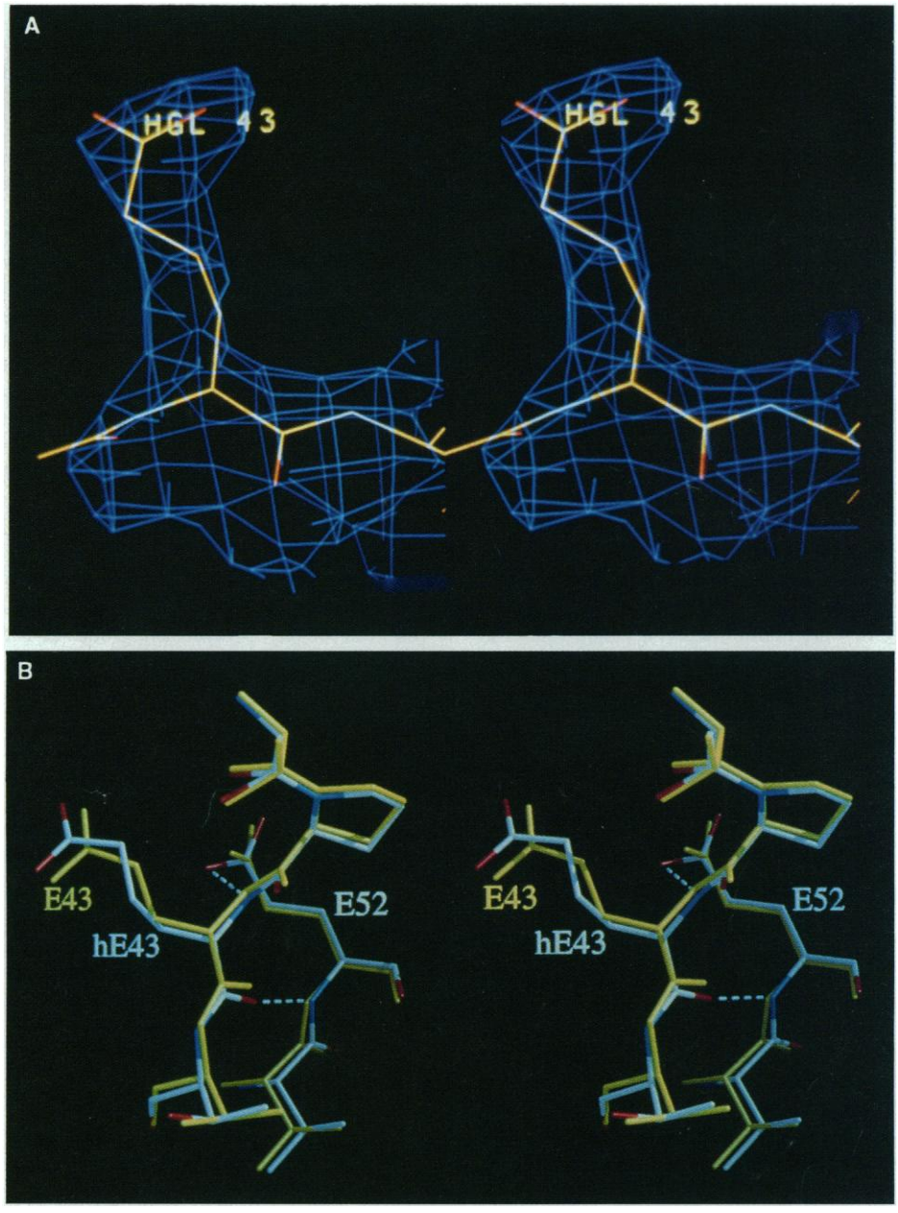

Fig. 4. (**A**) Difference electron density for residues 43 and 44, with the final model superimposed for comparison. Until this stage in the structure determination, loop residues 43 to 50 had been excluded from the model. $ADPA^{43}$ SNase was crystallized under conditions similar to those previously described (*2*), except that the protein concentration was 1.5 mg/ml and the MPD concentration in the reservoir solution was 40% (w/v). Diffraction data to 2.4 Å resolution were collected from five crystals ($P4_1$, a = 48.3 Å and c = 64.0 Å) with the use of a MAR image plate system at the Stanford Synchrotron Radiation Laboratory. The 23,935 measurements of 5960 unique reflections were merged with R = 8.9%, resulting in a data set that is 98% complete between 8 and 2.4 Å. Inspection of electron density maps calculated after rigid-body refinement with the inhibited wild-type structure (*2*) as the starting model revealed that no inhibitor was present in the active site, that the conformations of the active site residues were as seen in apo (*19*) rather than in inhibited SNase, and that density for loop residues 43 to 50 was poor. The model was adjusted accordingly, and cycles of refinement with XPLOR (*28*) and manual adjustment using FRODO (*29*), followed by introduction of water molecules, resulted in a final R factor of 18.7% (8 to 2.4 Å, 5533 reflections with $F > 0$). The final model consists of residues 6 to 45 and 51 to 141, together with 65 water molecules, and has good stereochemistry, as evidenced by rms deviations in bond lengths and angles of 0.008 Å and 1.7°, respectively. The final electron density map shows good density for all residues, with the exception of the termini and the loop residues 44 to 50. Residues 44 and 45 were placed into poor density, and residues 46 to 50 could not be built into the model, although there are patches of density consistent with the apo wild-type structure. The strongest features in the final difference map are four to five rms peaks corresponding to the phosphate moieties of the bound inhibitor in wild-type SNase. It is unclear whether these represent low-occupancy inhibitor or bound phosphate ions; nothing was built into this density. (**B**) Comparison of $ADPA^{43}$ SNase (residue labeled hE43; carbon atoms in white, nitrogen atoms in blue, and oxygen atoms in red) to the apo wild-type structure (all atoms in yellow) (*19*) in the region of residue 43. The torsion angles for the side chain of $ADPA^{43}$ are −88°, 111°, 80°, and −151°. The hydrogen bonds shown in this figure are found between O of 43 and N of 52 (2.68 Å) and between N of 43 and Oε1 of 52 (2.77 Å).

of the nitro and homoglutamate mutants makes this unlikely. Thus, it appears that a basic residue at position 43 is not required for high catalytic activity; only a bidendate hydrogen bond acceptor (a role not fulfilled by either glutamine or AHPA) is necessary.

The homoglutamate mutant also retains wild-type catalytic activity at pH 9.9, in contrast to the Glu^{43}→Asp mutant, in which V_{max} is reduced 300-fold. Both substitutions conserve charge but alter side chain geometry and steric interactions. In order to understand the mechanism by which the enzyme accommodates the additional methylene group in the homoglutamate side chain, we determined the x-ray crystal structure of this mutant to 2.4 Å resolution (Fig. 4). The structure of $ADPA^{43}$ SNase is very similar to that of wild-type apo, with a root-mean-square (rms) difference between backbone atoms of 0.2 Å. The largest differences (0.4 to 0.8 Å) occur in residues 42 to 51, 84 to 86, and 113 to 115. Differences in residues 42 to 51 and 113 to 115 have been observed between wild-type apo and inhibited structures (*19*), implying inherent flexibility in these regions. The extra methylene group of the homoglutamate side chain is accommodated by a 0.4 Å shift in the backbone of residue 43, accompanied by an adjustment of its side chain torsion angles (Fig. 4B). The net effect of these differences is that the homoglutamate carboxylate group moves to within 0.5 Å of the Glu^{43} carboxylate group in the apo wild-type structure, while maintaining a similar orientation with respect to the active site. This suggests that whatever role the side chain of Glu^{43} plays during catalysis can be fulfilled by the homoglutamate side chain. Furthermore, two hydrogen bonds between $ADPA^{43}$ and Glu^{52} are maintained (Fig. 4B). The Glu^{43} and Glu^{52} residues shift down slightly, but maintain the hydrogen bond between the side chain of Glu^{52} and the main chain amide of Glu^{43}, an interaction that may be important in preorganizing the adjacent Ω-loop (residues 43 to 52) for function during binding or catalysis.

Although both the nitro and homoglutamate mutants retain high activity at pH 9.9 (where the enzyme is typically assayed), they are less active than the wild-type enzyme at lower pH values (Fig. 3B). The difference in pH behavior may reflect different rate-determining steps in the mutant and wild-type enzymes. Recent studies (*20*) have shown a viscosity dependence on V_{max} for the wild-type enzyme above pH 7.3, suggesting that product release is rate limiting under these conditions. In contrast, a chemical step may be rate limiting in the two mutants described here (*21*). The pH dependence of V_{max} observed for the NABA and ADPA mutants is qualitatively similar to those reported for the Glu^{43}→Asp mutant (although the absolute activity of this mutant is reduced 300-fold) and a mutant in which residues 44 to 49 have been deleted (*20*). This similarity suggests that differences in loop geometry may be responsible for the observed decreases in rate. The hydrogen bonds between the carboxylate group of residue 43 and the main chain amides of residues 45 and 46 in the inhibited wild-type structure (*2*) may be important for fixing the loop into optimal position for catalysis. In the Glu^{43}→Asp mutant, these hydrogen bonds were absent, and the structure of the loop was substantially altered (*5*). The nitro analog of glutamate has only weak hydrogen-bonding properties (*22*), and the position of the homoglutamate carboxylate group differs from that of the wild type by 0.5 Å. Therefore, in each case the necessary hydrogen bonds may not be formed effectively.

Substitution of either Arg^{35} or Arg^{87} with the charged, monodentate hydrogen-bonding analog, AEHC, led to at least a 10^3-fold loss in catalytic activity at pH 7.5. The ammonium ion of AEHC (in contrast to that of Lys) should be able to occupy very nearly the same position as the terminal guanidinium-NH_2 group of Arg in the enzyme active site. Although the pK_a of AEHC is predicted to be one unit lower than that of lysine (*23*), it should be present predominantly in the charged form under the assay conditions. In the absence of any structural perturbations, these results, and the fact that the neutral isosteric CIT mutants also had 10^3-fold decreased activity, suggest that neither Arg^{35} nor Arg^{87} functions via simple electrostatic stabilization of the transition state or by protonation of the 5′-hydroxyl group of the substrate. It appears that both charge and bidentate hydrogen-bonding ability are critical features of these residues, consistent with a previous mechanistic proposal that both guanidinium groups shift to bidentate interactions in the transition state (*24*).

REFERENCES AND NOTES

1. F. A. Cotton, E. E. Hazen, J. J. Legg, *Proc. Natl. Acad. Sci. U.S.A.* **76**, 2551 (1979).
2. P. J. Loll and E. E. Lattman, *Proteins* **5**, 183 (1989).
3. S. Mehdi and J. A. Gerlt, *J. Am. Chem. Soc.* **104**, 3223 (1982); B. M. Dunn, C. DiBello, C. B. Anfison, *J. Biol. Chem.* **248**, 4769 (1973); E. H. Serpersu, D. Shortle, A. S. Mildvan, *Biochemistry* **26**, 1289 (1987); D. J. Weber, A. K. Meeker, A. S. Mildvan, *ibid.* **30**, 6103 (1991); D. J. Weber, E. H. Serpersu, D. Shortle, A. S. Mildvan, *ibid.* **29**, 8632 (1990); E. H. Serpersu, D. Shortle, A. S. Mildvan, *ibid.* **25**, 68 (1986).
4. D. W. Hibler *et al.*, *Biochemistry* **26**, 6278 (1987).
5. P. J. Loll and E. E. Lattman, *ibid.* **29**, 6866 (1990).
6. J. A. Wilde *et al.*, *ibid.* **27**, 4127 (1988).
7. T. Pourmotabbed, M. Del Acqua, J. A. Gerlt, S. M. Stanczyk, P. H. Bolton, *ibid.* **29**, 3677 (1990).
8. E. M. Arnett, *Prog. Phys. Org. Chem.* **1**, 223 (1963).
9. C. J. Noren, S. J. Anthony-Cahill, M. C. Griffith, P. G. Schultz, *Science* **244**, 182 (1989).
10. J. A. Ellman, D. Mendel, C. J. Noren, S. J. Anthony-Cahill, P. G. Schultz, *Methods Enzymol.* **202**, 301 (1991).
11. The polymerase chain reaction was used to delete the *ompA* leader sequence and to introduce an Nde I restriction site at the 5′-terminus of the SNase structural gene encoded in the plasmid pONF1 [M. Takahara *et al.*, *J. Biol. Chem.* **260**, 2670 (1985)] and a Xho I site at the 3′ end of the structural gene. The Nde I–Xho I fragment was then subcloned into pSAL127 (*12*), placing the SNase gene under the transcriptional control of the T7 promoter in the resulting vector, pKJSN1.
12. S. A. Lesley, Promega Corp., 2800 Woods Hollow Rd., Madison, WI 53711, unpublished results.
13. An Eco RI digest of pKJSN1 provided a 589–base pair fragment containing the gene for SNase and the T7 promoter region. This fragment was subcloned into M13mp18, and mutagenesis was done according to the Eckstein protocol [J. R. Sayers, W. Schmidt, F. Eckstein, *Nucleic Acids Res.* **16**, 791 (1988)]. Each mutant gene was sequenced in its entirety. The mutant SNase genes along with the T7 promoter were then cloned into the unique Eco RI site in pUC18 to provide pUCSN.E43am, pUCSN.R87am, and pUCSN.R35am.
14. A chromogenic plate assay [D. Shortle, *Gene* **22**, 181 (1983)] was used to screen for catalytically active mutants. In our experiments, 2 μl of the cleared supernatants from a 30-μl in vitro protein synthesis reaction were spotted on a plate containing 1% agar, 1% NaCl, 50 mM sodium glycinate (pH 9.9), 20 mM $CaCl_2$, single-stranded calf thymus DNA (100 μg/ml), and toluidine blue O (0.2 mg/ml). After incubation for 2 hours at 37°C, catalytically active SNase was identified by the presence of a pink halo against the blue background. When the suppressor tRNA was omitted from or supplied in unacylated form to the in vitro reaction, no full-length protein was produced (data not shown), and no catalytic activity could be observed. In experiments where mock in vitro reactions (containing all of the components except the expression vector) were spiked with known amounts of purified SNase, amounts of wild-type SNase as low as 5 pg/μl produced a detectable halo. Upper limits on readthrough or mutant catalytic activities were then calculated on the basis of an expression level of 20 μg/ml. From this analysis, we estimate that as little as 0.025% readthrough of the TAG codon that resulted in a protein of wild-type activity could have been detected. These controls demonstrate that the in vitro system does not contain endogenous suppressor tRNAs capable of reading through the amber stop codon, and that the aminoacyl tRNA synthetases present in the *Escherichia coli* S-30 extract do not aminoacylate the suppressor $tRNA_{CUA}$ with any of the 20 natural amino acids.
15. A 5-ml in vitro protein synthesis reaction was treated with 100 μl of polyethylenimine hydrochloride (pH 7.5) and centrifuged. The cleared supernatants were loaded onto a carboxymethyl-cellulose cation exchange column with 50 mM tris-HCl (pH 7.5) and eluted with a 0 to 2 M NaCl gradient in that buffer. Fractions containing nuclease activity were lyophilized, dialyzed against 50 mM sodium acetate (pH 4.9), 1 mM EDTA, then loaded onto a Mono-S column (Pharmacia) and eluted with a 0 to 1 M NaCl gradient. Fractions containing nuclease activity were pooled and determined to be more than 95% homogenous by silver-stained SDS–polyacrylamide gel electrophoresis (PAGE) analysis.
16. The assay mixture contained 40 mM sodium glycinate (pH 9.9), single-stranded calf thymus DNA (75 μg/ml) in which the concentration of Ca^{2+} was varied between 0.3 and 3.6 mM in a volume of 1.0 ml at 25 ± 1°C. The assay mixture was determined to contain saturating amounts of DNA by the observation of indistinguishable rates at 75

and 90 μg per milliliter of DNA. We used similar plots to determine the apparent V_{max} and K_m^{DNA} values by varying the concentration of DNA from 7 to 50 μg/ml in 40 mM sodium glycinate (pH 9.9) with 10 mM Ca^{2+} (data not shown). Reactions were initiated by the addition of 20 ng of protein, and we determined the initial velocities by monitoring the increase in absorbance at 260 nm (A_{260}). The numbers reported represent the standard deviations of three data collections obtained for each protein on the same day. Protein concentrations were initially determined by SDS-PAGE analysis of ^{35}S-methionine–labeled samples of wild-type and mutant SNase. The wild-type band was excised and quantitated by scintillation counting; the remaining wild-type sample was assayed for catalytic activity, and the known specific activity was used to determine the concentration (in micrograms per milliliter) of wild-type SNase present. Quantitation of the gel slices containing mutant proteins by scintillation counting was followed by catalytic assay to provide the specific activity of each mutant in units of ΔA_{260} min^{-1} μg^{-1} SNase. For the pH versus rate profiles, assays were done as described above, at 10 mM Ca^{2+} and at DNA concentrations ranging from 6 to 80 μg/ml. Between pH 7.5 and 8.5, 40 mM tris-HCl was used as the buffer; from pH 8.5 to 9.9, assay mixtures were buffered with 40 mM sodium glycinate. Duplicate data points were gathered for each concentration of DNA at each pH; points on the pH versus rate plot represent the average value of two (NABA and ADPA) or three (wild type) of such sets of data. The lines were fit by linear least squares analysis; no weighting was performed.

17. P. Cuatrecasas, S. Fuchs, C. B. Anfinsen, *J. Biol. Chem.* **242**, 1541 (1967).
18. C. D. Slater, *J. Org. Chem.* **46**, 2173 (1981).
19. T. R. Hynes and R. O. Fox, *Proteins* **10**, 92 (1991).
20. S. P. Hale, L. B. Poole, J. A. Gerlt, *Biochemistry*, in press.
21. Both mutants (Glu^{43}→NABA and Glu^{43}→ADPA) and the wild-type enzyme exhibited a significant kinetic isotope effect in D_2O, with V_{max}^H/V_{max}^D = 2 to 3. The solvent isotope effects observed here suggest that chemical steps contribute to the rate-determining step in both the wild type and the mutants; chemistry and loop movement may be coupled, as was recently observed for triosephosphate isomerase (*25*). Kinetic isotope effects were determined as described [R. L. Schowen, in *Isotope Effects on Enzyme Catalyzed Reactions*, W. W. Cleland, M. H. O'Leary, D. B. Northrop, Eds. (University Park Press, Baltimore, MD, 1977), pp. 64–99]. Concentrated buffer stocks (400 mM sodium glycinate) were prepared by addition of solid glycine to H_2O or D_2O and adjustment of the pH with 6 N NaOH (in D_2O, pD = pH + 0.4); the final H_2O content in the D_2O buffers was less than 10% (v/v) after this procedure. Assay buffers were then prepared by dilution of stock solutions into H_2O or D_2O. Values of V_{max} were obtained from Lineweaver-Burk plots of two sets of kinetic data for each protein: for pH or pD values from 9.4 to 10.4, assay buffers contained 40 mM NaGly, 10 mM Ca^{2+}, and 10, 20, 40, or 80 μg of DNA per milliliter; for pD values above 10.4, buffers contained 40 mM NaGly, 10 mM Ca^{2+}, and 80, 100, or 120 μg of DNA per milliliter. The kinetic isotope effects were estimated from the differences in maximal values of V_{max}, which were observed at pH 9.9 in H_2O and pD 10.4 (Glu^{43}→NABA) or 10.6 (wild type and Glu^{43}→ADPA) in D_2O. By monitoring the intrinsic fluorescence of Trp^{140} [D. Shortle and A. M. Meeker, *Proteins* **1**, 81 (1986)] as a function of pH or pD, we have determined the midpoint for denaturation of wild-type SNase to be at pH 10.4 in H_2O and pD 11.2 in D_2O. As such, we do not believe that denaturation effects complicate our analyses.
22. M. D. Joesten and L. J. Schaad, *Hydrogen Bonding* (Dekker, New York, 1974), pp. 309–335.
23. P. Hermann and K. Lemke, *Hoppe-Seyler's Z. Physiol. Chem.* **349**, 390 (1968).
24. D. J. Weber *et al.*, *Proteins* **13**, 275 (1992).
25. N. S. Sampson and J. R. Knowles, *Biochemistry* **31**, 8488 (1992).
26. D. J. Suich, thesis, University of California, Berkeley (1993).
27. CIT and ADPA (L-α-aminoadipic acid) (both from Sigma) were protected for chemical aminoacylation reactions as described (*10*). AEHC was obtained from the reaction of *N*-NVOC (nitroveratryloxycarbonyl)-1-bromo-2-aminoethane with the sodium salt of *N*-NVOC-L-homocysteine. NABA and AHPA were first synthesized by D. J. Suich (*26*).
28. A. T. Brunger, *XPLOR Manual* (Yale Univ. Press, New Haven, CT, version 3.1, 1992).
29. A. T. Jones, *J. Appl. Crystallogr.* **11**, 268 (1978).
30. Plasmid pONF1 was provided by J. A. Gerlt, University of Maryland. We thank D. Mendel for assistance in developing the purification protocol for SNase, A. Kossiakoff for helpful discussions, and J. Gerlt for comments on this manuscript and for sharing data before publication. We are grateful for financial support of this work from the National Institutes of Health (grant ROI GM-49220). J.K.J. was supported by an NIH Postdoctoral Fellowship (GM 14012-02S1) and T.R.G. by an NIH Biotechnology Training grant (T32GM-08388). P.G.S. is a W. M. Keck Foundation Investigator.

16 February 1993; accepted 15 July 1993

Thymic Selection of Cytotoxic T Cells Independent of CD8α-Lck Association

Iris T. Chan, Andreas Limmer, Marjorie C. Louie, Eric D. Bullock, Wai-Ping Fung-Leung,* Tak W. Mak, Dennis Y. Loh†

The CD8α cytoplasmic domain associates with $p56^{lck}$, a nonreceptor protein–tyrosine kinase. The biological relevance of CD8α-Lck association in T cell development was tested with transgenic mice generated to express a CD8α molecule with two amino acid substitutions in its cytoplasmic domain, which abolishes the association of CD8α with Lck. The CD8α mutant was analyzed in a $CD8^{-/-}$ background and in the context of the transgenic 2C T cell receptor. The development and function of $CD8^+$ T cells in these mice were apparently normal. Thus, CD8α-Lck association is not necessary for positive selection, negative selection, or CD8-dependent cytotoxic function.

During the course of thymic development, selection events occur in the thymus to eliminate self-reactive T cells (negative selection) and retain T cells reactive to foreign antigens (positive selection) (*1*). Among the cell surface molecules involved in these processes are the T cell receptor (TCR) and CD8 or CD4 glycoproteins on the T cells and the major histocompatibility complex (MHC) proteins bound to antigenic peptides on antigen-presenting cells in the thymus. T cell precursors are initially $CD4^-CD8^-TCR^-$ double negative (DN) but differentiate to a $CD4^+CD8^+TCR^{lo}$ double positive (DP) stage. These DP cells are thought to be susceptible to selection. Mature T cells that are positively selected are phenotypically $CD4^+CD8^-$ or $CD4^-CD8^+$ single positive (SP).

The CD8 surface glycoprotein is involved in the outcome of thymic selection (*2–4*). In mouse thymocytes, CD8 is a disulfide-linked homodimer of 38-kD α (Lyt2) chains or a heterodimer of α and 30-kD β (Lyt3) chains. In peripheral T cells, CD8 occurs predominantly as an αβ heterodimer (*5*). CD8 functions as an adhesion molecule by binding to the nonpolymorphic α3 domain of MHC class I molecules. CD8 may also function in intracellular signal transduction, because the cytoplasmic domain of CD8α associates noncovalently with $p56^{lck}$, a Src family nonreceptor tyrosine kinase (*6*). Substitution of two cysteines in the CD8α cytoplasmic domain with alanine or serine residues abolishes its association with Lck (*7, 8*).

To assess the role of CD8α-Lck association during T cell development, we analyzed transgenic mice that contained mutations at the two cysteines in the CD8α cytoplasmic domain ($CD8^{CA}$). Peripheral blood T lymphocytes from the founders ($CD8^{CA}8^{+/+}$) demonstrated only $CD4^+CD8^+$ and $CD4^-CD8^+$ cells. The $CD4^+CD8^+$ population consisted of cells that would normally have been $CD4^+$ but now expressed the $CD8^{CA}$ transgene; no $CD4^+CD8^-$ cells were found in the peripheral blood of these mice (*9*). In the founder lines analyzed, $CD8^{CA}$ transgene expression was two to three times that of endogenous CD8α. To study the effects of the $CD8^{CA}$ mutation without endogenous wild-type CD8 molecules, we mated $CD8^{CA}$ mice to CD8-deficient mice [$CD8^{-/-}$ (*3*)] to obtain $CD8^{CA}8^{-/-}$ mice (*10*). The

I. T. Chan, A. Limmer, M. C. Louie, E. D. Bullock, D. Y. Loh, Howard Hughes Medical Institute, Department of Medicine, Genetics, and Molecular Microbiology, Washington University School of Medicine, St. Louis, MO 63110.
W.-P. Fung-Leung and T. W. Mak, Ontario Cancer Institute and Departments of Medical Biophysics and Immunology, University of Toronto, Ontario M4X 1K9, Canada.

*Present address: R. W. Johnson Pharmaceutical Research Institute, Don Mills, Ontario M3C 1L9, Canada.
†To whom correspondence should be addressed.